

Measurements of Wall Heat Flux and Temperature in a Supersonic Model Combustor

Long Li¹, Xuejun Fan² and Jing Wang³

Institute of Mechanics, Chinese Academy of Sciences, Beijing, 100190, P. R. China

In this paper, an integrated water-cooled sensor has been developed to simultaneously measure the heat flux and temperature at the wall of a scramjet combustor. The sensor was designed based on the principle of Gardon heat-flux gauge. Numerical simulation of the heat conduction processes inside the sensor has been carried out to obtain the time responses of the sensor. Calibration processes using radiative and conductive heating sources were carried out and calibration curves such as heat flux vs. output voltage and wall temperature vs. heat flux were obtained. The effects of structural material and dimensions on the sensor's responses have also been examined. Several wall heat flux/temperature sensors have been built and tested in a Mach 2.5 supersonic combustor at stagnation temperatures up to 1920 K and the results demonstrate satisfactory time response and stability of the sensor.

Nomenclature

α	=	thermocouple coefficient
E	=	output voltage of heat flux sensor
Q	=	heat flow
q	=	heat flux
R	=	heat resistance
σ	=	Stefan-Boltzmann constant in thermal radiative heat transfer
T_b	=	temperature of the heat sink or sensor base
T_{bc}	=	temperature of blackbody cavity
T_{BN}	=	temperature at the center of BN ceramic disk
T_c	=	temperature at the center of constantan disk
T_i	=	initial temperature of the numerical simulation field

I. Introduction

Wall heat flux and temperature are the key parameters for designing the thermal protection system of a scramjet combustor. Measurements of wall heat flux and temperature become very difficult at high flight Mach number because the sensors will face extremely hostile environment due to the excessive heat release from aerodynamic heating and combustion. For example, at flight Mach number above 6, the total temperature of air after combustion will exceed 2800 K and the average wall heat flux in the combustor ranges from 1.0 to 5.0 MW/m² depending on the fuel used. Besides, the high temperature gases are also rich in oxygen, which will oxidize the sensor materials very quickly. The common sensor structure and materials could not last very long time in such an environment and active cooling is usually required to protect the sensors.

The wall heat flux is usually measured using sensor techniques based on (1) spatial temperature gradient such as Schmidt-Boelter heat flux meter^{1,2} and Gardon heat flux meter^{3,4}; (2) temperature variation of a subject with time^{5,6}; (3) Surface heating⁷ (hot-film). The sensor based on spatial temperature gradient has a good sensitivity but limited range of measurement of approximately 0.1 MW/m². The measurement range of this type of sensor could be extended greatly using a bypass heat flow path with active cooling. However, the measurement sensitivity will become very low and the time response will become very long if the heat resistances of the two heat flow paths are

¹ PHD Student, National Key Laboratory of High Temperature Gas Dynamics, lli918@126.com.

² Professor, National Key Laboratory of High Temperature Gas Dynamics, xfan@imech.ac.cn, Member AIAA.

³ Assistant Professor, National Key Laboratory of High Temperature Gas Dynamics, wangjing@imech.ac.cn.

ill-matched. The sensor based on temperature history has a much larger measurement range of order of 10 MW/m² but can only work for a few milliseconds. The accuracy of this type of sensors is also unsatisfactory. For example, the wall heat flux of HyShot II Scramjet combustor measured in the High Enthalpy Shock Tunnel Gottingen (HEG)^{8,9} had an uncertainty of approximately 50%.

Another difficulty related to the heat flux measurement is the sensor calibration. There are various calibrations methods^{10,11}, among which the blackbody cavity¹² is the most practical one. Heat flux calibrated up to 5 W/cm² were obtained with the sensor placed outside a blackbody cavity¹³⁻²². Calibrations of water-cooled sensors placed inside blackbody cavity have been tested recently and maximum heat flux up to 50 W/cm² and 100 W/cm² were obtained by Murthy at NIST^{23,24} and Abdelmessih at Saint Martin's University²⁵, respectively.

This paper is aimed to develop a high temperature sensor used to simultaneously measure the wall heat flux and temperature. The sensor was designed based on principle of Gardon heat flux gauge. Recirculating water was used to cool down the sensor structure. The protection shell of the sensor was also used as a bypass heat flow path to extend the measurement range. Heat resistance analysis and numerical simulation have been carried out to help the design and optimization of the sensor structure. Calibration processes of the sensor using radiative and conductive heating were described in detail. Finally, Preliminary results of the sensors tested in a Mach 2.5 Scramjet combustor were given and compared at various stagnation temperatures up to 1920K.

II. Design of high temperature wall heat flux sensor

The heat flux sensor is designed based on the Gardon heat flux gauge²⁶. The Gardon gauge consists of a thin circular constantan disk, a copper heat sink and a copper wire at the center of the constantan disk as shown in Fig. 1. The constantan disk was well welded at the edge of the copper heat sink. The slender copper wire, as positive electrode of output signal, was welded at the disk center. Another copper wire, as negative electrode, was connected to the copper heat sink. According to the thermocouple principle, the output voltage E is proportional to the temperature difference between the center and the edge of the constantan disk. The temperature difference is also proportional to the heat flux q applied normal to constantan disk²⁶:

$$E = \alpha(T_c - T_b) = C \cdot q \quad (1)$$

where α is the thermocouple coefficient and C is a constant for calibration.

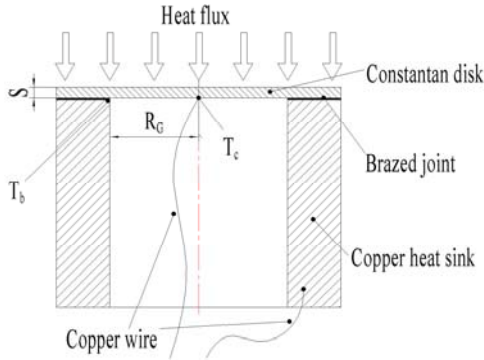


Fig. 1 Schematic of the Gardon heat flux gauge.

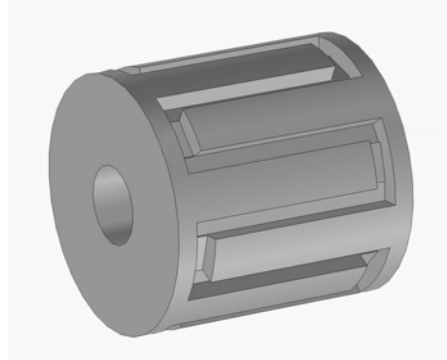


Fig. 2 The structure of cooling channels in the copper heat sink.

To design a high temperature heat flux sensor, the copper heat sink of the Gardon gauge is cooled down using recirculating water. Fig. 2 shows the S-shaped cooling channels structure used in the present study. A boron nitride (BN) ceramic disk is glued on the top of the constantan disk to protect it from high temperature gases as shown in Fig. 3. The BN ceramic is machinable and has excellent electric insulation, thermal conductivity. Its using temperature can reach at 2800°C in inert gas but should be kept below at 1000°C when oxygen presents. The whole gauge is inserted tightly into a cylindrical metal shell. This metal shell is also used to bypass part of the heat flow received from the sensor head in Fig. 3.

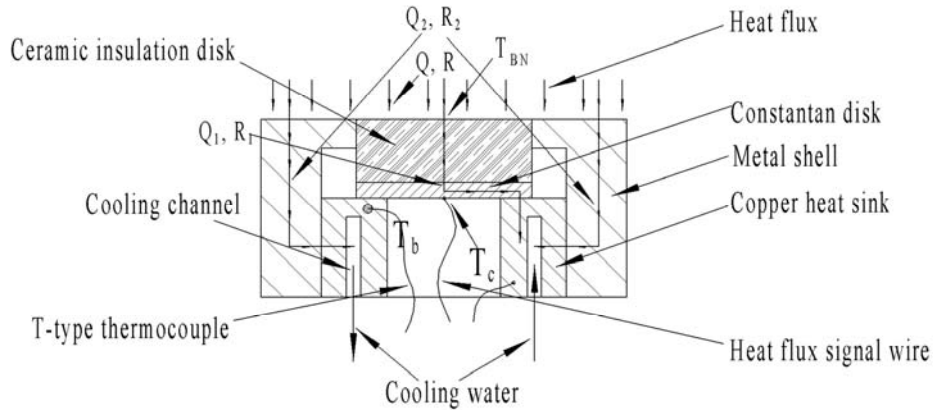


Fig. 3 Schematic of the present heat flux sensor

With a bypass heat flow path, the measurement range of the sensor will be extended significantly. The total heat flow received from the sensor head in Fig. 3 will be divided into two branches: the first Q_1 flows through the ceramic and constantan disks, the second Q_2 flows through the metal shell, and both of them converge at the copper heat sink. Assuming the heat resistances of two paths, R_1 and R_2 , connected in parallel, $Q_2 \gg Q_1$ when $R_2 \ll R_1$, and little heat will flow through the constantan disk and the output signal is weak; on the contrary, $Q_2 \ll Q_1$ when $R_2 \gg R_1$, and most of heat will flow through the constantan disk. In the following section, numerical simulation of the heat conduction processes inside the sensor structure will demonstrate that the output signal of the Gardon gauge is proportional to the total heat flux received from the sensor. Consequently, measurements of much higher levels of heat flux can be made using the sensor designed in Fig. 3, and its measurement range can be adjusted conveniently by varying the ratio of two heat resistances of R_1 and R_2 .

III. Numerical simulation of heat conduction in the sensor structure

Numerical simulation has been performed to study the heat conduction processes inside the constantan disk and the whole heat flux sensor. Table 1 lists the materials and their physical properties used in the simulation.

Table 1 Physical properties of materials used in simulation

Component	Material	Density, $\times 10^3$ kg/m^3	Thermal conductivity, $\text{W/m}^2\text{K}$	Specific heat capacity, $\text{J/kg}\cdot\text{K}$
Insulation disk	Boron nitride	2.3	30	1600
Gardon gauge	Constantan	8.9	22	400
sensor shell, heat sink	Copper	8.0	400	400

A. Numerical simulation of heat conduction inside the constantan disk

The heat conduction process inside the constantan disk of a Gardon gauge has been simulated using ANSYS 12 solver with uniform heat flux applied normal to its top surface as shown in Fig. 4.

The Constantan disk has a diameter of 12 mm and a thickness of 0.1 mm. Boundary conditions of constant temperature at 300K at the edge of the disk and adiabatic at the bottom surface is assumed, and initial condition of uniform temperature distribution ($T_i=300\text{ K}$) is used in the simulation.

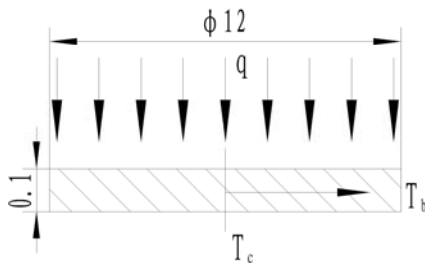


Fig. 4 Computation model of the constantan disk, all dimensions in mm.

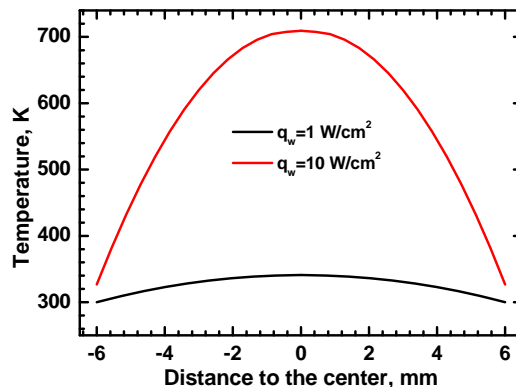


Fig. 5 Steady state temperature distributions on the top surface of constantan disk for two different heat fluxes.

Fig. 5 shows the steady state temperature distributions on the top surface of the constantan disk for heat flux q of 1.0 W/cm^2 and 10 W/cm^2 . The calculated temperature difference between the top and bottom surfaces is very small, approximately 0.02 K for applied heat flux of 1 W/cm^2 , which indicates that the vertical thermal conduction can be neglected and one dimensional heat conduction assumption can be used in designing the Gardon gauge.

Fig. 6 shows the temperature response at the top center of constantan disk when a heat flux of 1 W/cm^2 is applied. It shows the temperature reaches a steady state after approximately 6 seconds. Fig. 7 shows the linear dependence of the steady state temperature at the center of constantan disk to the applied heat flux. It can also be seen that the maximum heat flux can be measured from this constantan disk is about 12 W/cm^2 corresponding to the maximum temperature of approximately 800 K for a T-type thermocouple according to the international standard²⁷.

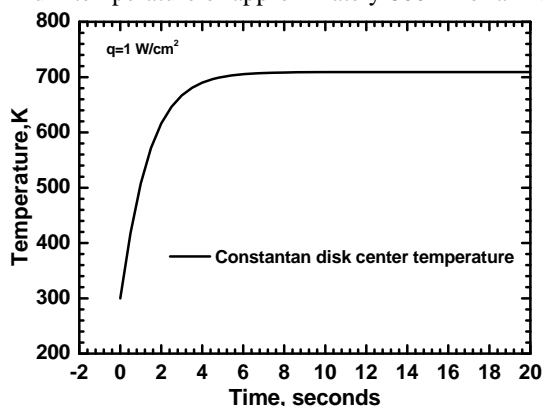


Fig. 6 Center temperature response curve of the constantan disk.

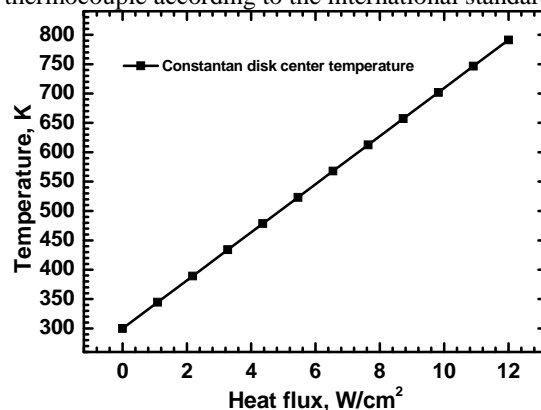


Fig. 7 Steady state temperature at the center of constantan disk as a function of applied heat flux.

B. Numerical simulation of heat conduction inside the heat flux sensor

A simplified computation model of the heat flux sensor corresponding to Fig. 3 is shown in Fig. 8. Constantan disk with the same dimension as in Fig. 4 is used. Copper is chosen as the shell material. The copper heat sink and the shell are assumed to at the same temperature of 300 K due to cooling and the initial temperature of the sensor is uniform at 300 K .

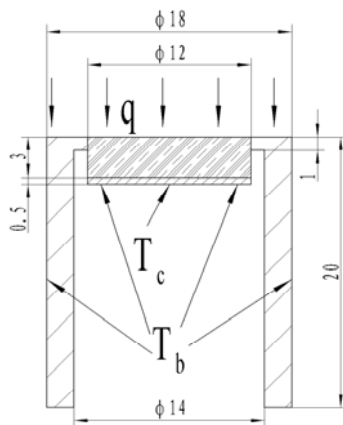


Fig. 8 Simplified computation model for the heat flux sensor in Fig. 3. All dimensions in mm.

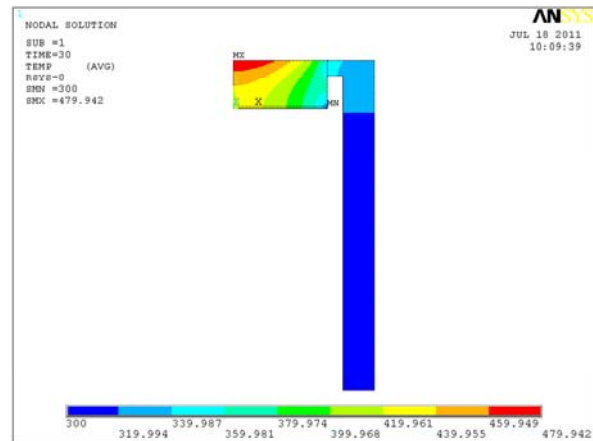


Fig. 9 Steady state temperature contour of the sensor.

Fig. 9 shows the steady state temperature contour of the simplified sensor model with a heat flux of $q=100$ W/cm². The maximum temperature is 480 K at the center of top surface of the ceramic disk.

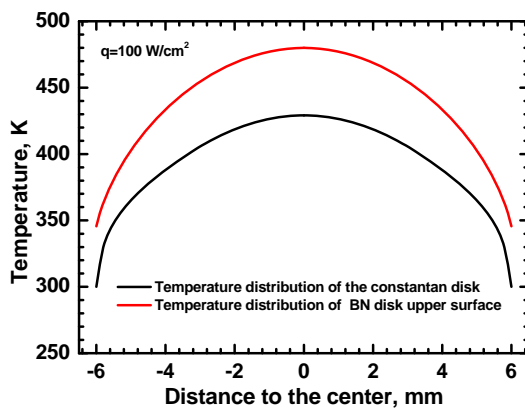


Fig. 10 Steady state temperature distributions at the top surface of constantan and BN ceramic disks.

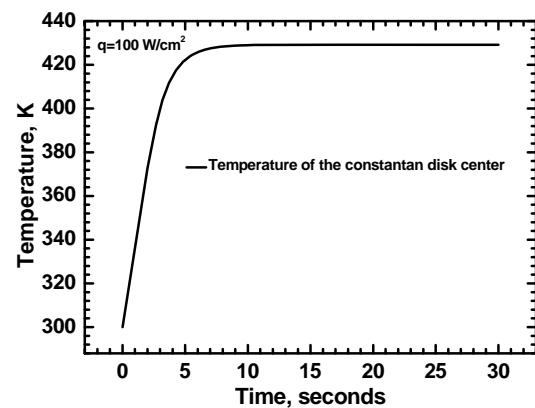


Fig. 11 Temperature response curve at the center of constantan disk.

Fig. 10 shows the steady state temperature distributions at the top surfaces of constantan and BN ceramic disks with a heat flux of 100 W/cm². Compared to Fig. 5 the temperature at the surface of Constantan disk becomes lower for the same heat flux due to the addition of copper shell and ceramic disk.

Fig. 11 shows the temperature response at the top center of the constantan disk when a heat flux of 100 W/cm² is applied. The response time is approximately 8 seconds, a little longer than that in Fig. 6.

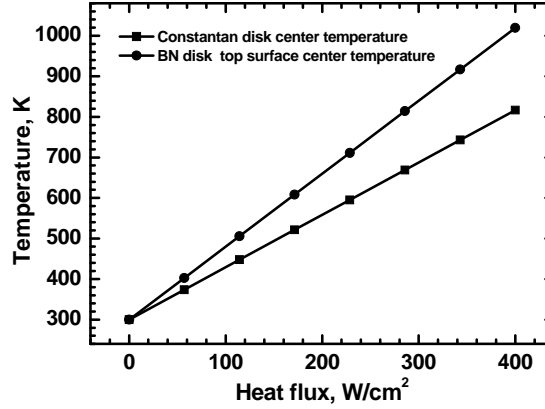


Fig. 12 Temperatures at the top centers of constantan and BN disks as a function of applied heat flux.

Fig. 12 shows the linear dependence of the steady state temperatures at the top centers of constantan and BN ceramic disks to the applied heat flux. . The two curves can be fitted linearly as following:

$$T_c = C_1 q + T_b \quad (2)$$

$$T_{BN} = C_2 q + T_b \quad (3)$$

where T_c is the temperature at the center of constantan disk, T_b is the temperature of copper heat sink, T_{BN} is the temperature at the center of BN ceramic disk, and C_1 and C_2 are the proportional constants. It can be seen from Fig. 12 that the maximum heat flux can be measured from this constantan disk is about 400 W/cm² corresponding to the maximum constantan temperature of approximately 800 K, which is much higher than the maximum heat flux of 12 W/cm² that a Gardon gauge can measure.

IV. Calibrations of the integrated heat flux and temperature sensor

Integrated wall heat flux and temperature sensors have been developed based on the numerical simulation in the previous section. Fig. 13 shows a picture of the sensor. Brass is used to make the thermal conduction shell. The diameters of the shell and the BN disk are 18 mm and 12 mm, respectively. More details of the sensor can be found in Fig. 3.

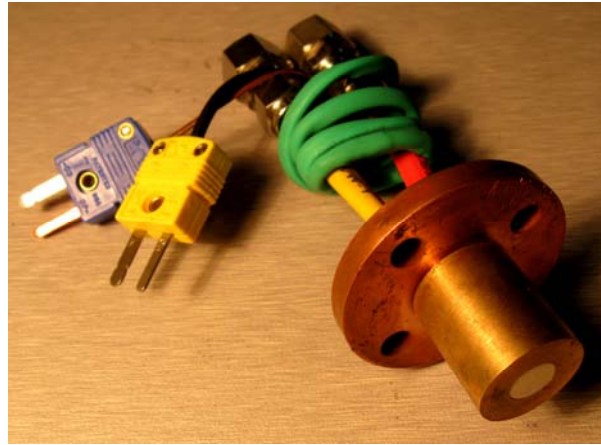


Fig. 13 Photograph of the integrated sensor for wall heat flux and temperature measurements.

A. Low heat flux calibration of the integrated sensor

The heat flux sensor was first calibrated using a radiation heating device consisting of 10 tungsten iodine lamps as shown in Fig. 14. The maximum power of each lamp is 2 kW. A standard commercial heat flux meter was used to calibrate the present sensor. The calibration result is plotted in Fig. 15. It can be seen from the figure that the

sensor's output voltage varies linearly with the applied heat flux. A sensitivity of $7.57 \text{ W/cm}^2\text{-mV}$ with a relative error of 1.7% was obtained from the calibration. The maximum heat flux limited by the power of lamps in the calibration was approximately 10 W/cm^2 . Calibration with higher heat flux using black body cavity will be described later.

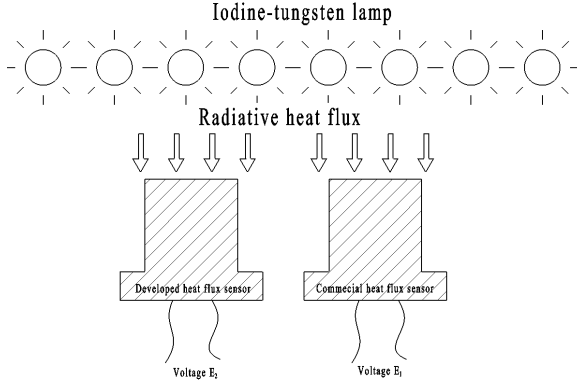


Fig. 14 Sensor calibration using Tungsten iodine lamps.

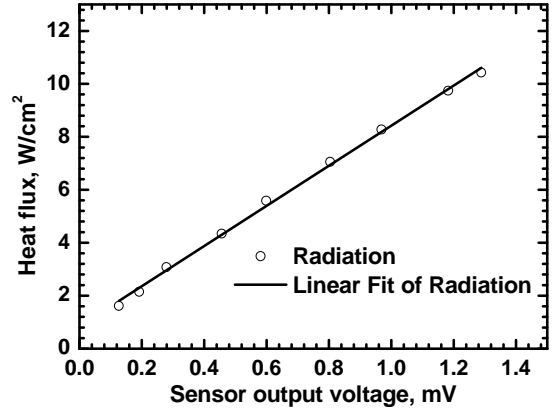


Fig. 15 Calibration curve of heat flux vs. sensor's output voltage.

B. Method to determine the top wall temperature of the heat flux sensor

In a Scramjet combustor the wall heat flux is closely related to the local wall temperature. Wall temperature should be measured simultaneously to obtain a meaningful measurements of the wall heat flux. The wall temperature in a scramjet combustor can reach 2000-3000 K and direct measurements of the wall temperature using common thermocouple become very difficult. However, the average wall temperature at the top surface of sensor can be obtained from the heat flux measurement if a correlation exists between them. As shown in Fig. 12, the measured heat flux q is proportional to the temperature difference between the top center of the BN ceramic disk and the copper base and according to equation(3):

$$q = C_2 (T_{BN} - T_b) \quad (4)$$

According to thermocouple Eqn. (1), Eqn. (4) can be written as

$$T_{BN} - T_b = C_3 \cdot E \quad (5)$$

where C_3 is a constant which can be calibrated by the measurements of T_{BN} , T_b and E .

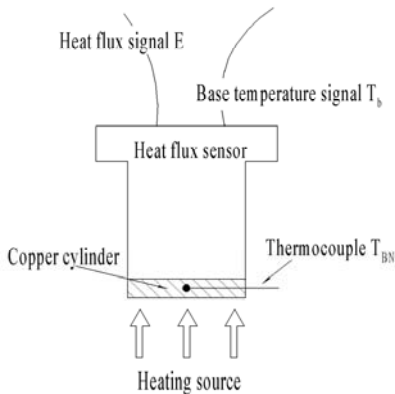


Fig. 16 Schematic of the wall temperature calibration device.

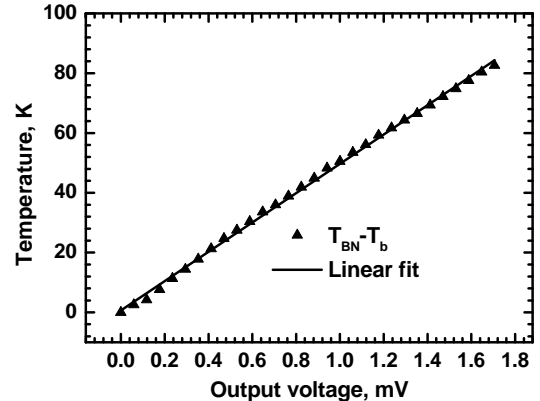


Fig. 17 Calibration curve of the temperature difference in Eqn. (4) vs. the sensor's output voltage.

Fig. 16 shows the calibration device for wall temperature. The wall temperature at the top of heat flux sensor is measured using a thermocouple inserted into a thin copper cylinder which was mounted tightly on the top of the sensor. An electric heating source was used to heat up the copper cylinder. The heat flux signal E , the base temperature T_b and the wall temperature T_{BN} were acquired simultaneously as the cylinder was heated up. Fig. 17

plots the variation of $T_{BN} - T_b$ with the output voltage of heat flux sensor. It shows a good linearity with the linear coefficient C_3 of approximately 49.1 K/mV with a relative error of 0.73%.

C. Effects of sensor materials and dimensions

There are many factors will affect the response characteristics of the heat flux sensor. Fig. 18 compares the response signals of heat flux sensors with different shell materials and insulation thickness. It can be seen from the figure that the bare sensor without any shell and insulator has the highest signal level and the fastest time response. Sensor with a copper shell has the fastest response time but the lowest signal level. When shells of aluminum, brass and stainless steel are used, the time response decreases and the signal level increases as material's conductivity decreases. On the other hand, the response signal level of the sensor with 2 mm BN insulation is approximately twice of that with 3 mm BN insulation.

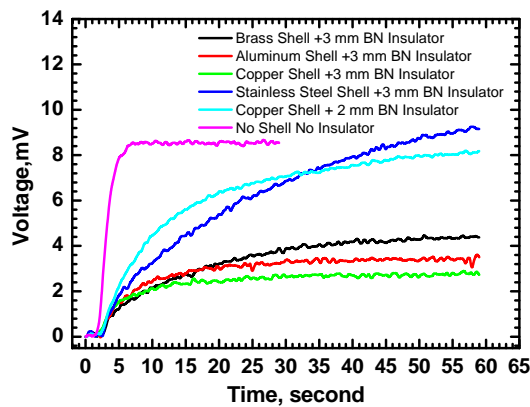


Fig. 18 Response signals for sensors with different structures.

D. Sensor calibration using black body cavity

To calibrate the sensor at high temperature and heat flux, a blackbody cavity calibration system has been designed and fabricated as shown in Fig. 19.

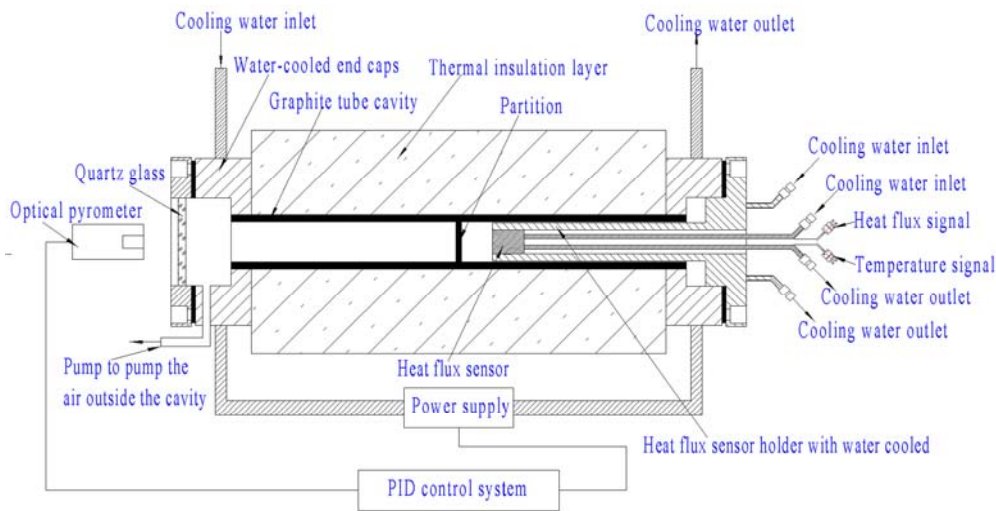


Fig. 19 Schematic of the blackbody cavity calibration system

The key component of the blackbody cavity is a graphite tube with an inner diameter of 30 mm and an outer diameter of 40 mm. The tube is divided equally into two cavities using a graphite disk of 5 mm in thickness, and is installed inside a stainless steel cylinder of 680 mm long and 400 mm in diameter. Thermal insulation material is

filled in the space between the graphite tube and the outside cylinder. Two brass flange brackets installed at the ends of the graphite tube, are used as the electrodes of the power supply. Circulating water is used to cool down the electrodes. A high temperature optical pyrometer with a measurement range of 750~3000 °C is used to monitor the cavity temperature through a quartz glass window install at the left end of the cavity. The output signal of the pyrometer is connected to a PID controlling system to control the heating power. The graphite tube is heated with a low voltage of 14 V and large current of more than 1000 A. Air is evacuated first and pure argon is filled into the cavity to prevent the structure from oxidation at high temperature. Temperature at the outlet of the graphite tube is lower than the center because of bracket cooling. The heat flux would be very small if the sensor is placed outside the graphite tube, which is on the order of 1.0 W/cm². To obtain a much higher heat flux, the sensor is inserted into the tube at a distance of 30 mm from the separation disk. Numerical simulation shows that there is an uniform temperature zone of 50 mm in length away from the separation disk. The sensor for calibration is protected from high temperature inside cavity using a water cooled sleeve made of stainless steel. The sleeve has an inner diameter of 18 mm and an outer diameter of 28 mm. Several BN ceramic rings of 20 mm in length and 1 mm in thickness are installed outside the sleeve to electrically insulate the sleeve from graphite tube. The top surface of the sensor is coated with soot to obtain an emissivity higher than 0.95 such that the heat flux applied to the sensor could be estimated using the law of blackbody radiation:

$$q = \sigma(T_{bc}^4 - T_{BN}^4) \quad (5)$$

where $\sigma=5.67 \times 10^{-8} \text{ W/m}^2 \cdot \text{K}^4$ is the Stefan-Boltzmann constant, T_{bc} is the temperature of blackbody cavity and T_{BN} is the temperature on the top surface of sensor. With water cooling the temperature T_{BN} is less than half of the temperature of blackbody cavity T_{bc} , thus $T_{BN}^4 \ll T_{bc}^4$, radiation heat flux could be approximated within an uncertainty of few percentage by:

$$q \sim \sigma T_{bc}^4 \quad (6)$$

The blackbody cavity can be heated from 750°C to 2500°C, which corresponds to a heat flux of 8~350 W/cm².

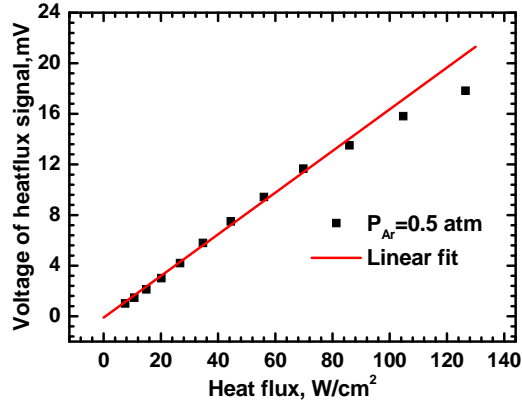


Fig. 20 Blackbody calibration curve for the heat flux sensor.

Fig. 20 shows the resulting calibration curve for the heat flux sensor. Linear dependence of the sensor's output voltage on the applied heat flux can be observed for the radiation heat flux less than approximately 100 W/cm². Deviation away from the linear fit occurs at higher heat flux level, which could be caused by the deformation of the sensor structure at high temperature and further study is needed. The calibration coefficient from Fig. 20 is approximately 0.164 mV/(W/cm²) with a relative error of 3%.

V. Measurements of the wall heat flux and temperature in a supersonic model combustor

Preliminary measurements were carried out in a Mach 2.5 supersonic model combustor (Fig. 21) with liquid kerosene injection at total temperatures of 1100-2000 K and total pressure of approximately 1.4 MPa. The combustor was cooled with recirculating water to make the experiment time longer than 200 seconds. Seven heat flux/ temperature sensors were installed along the centerline of the top combustor wall as shown in Fig. 21.

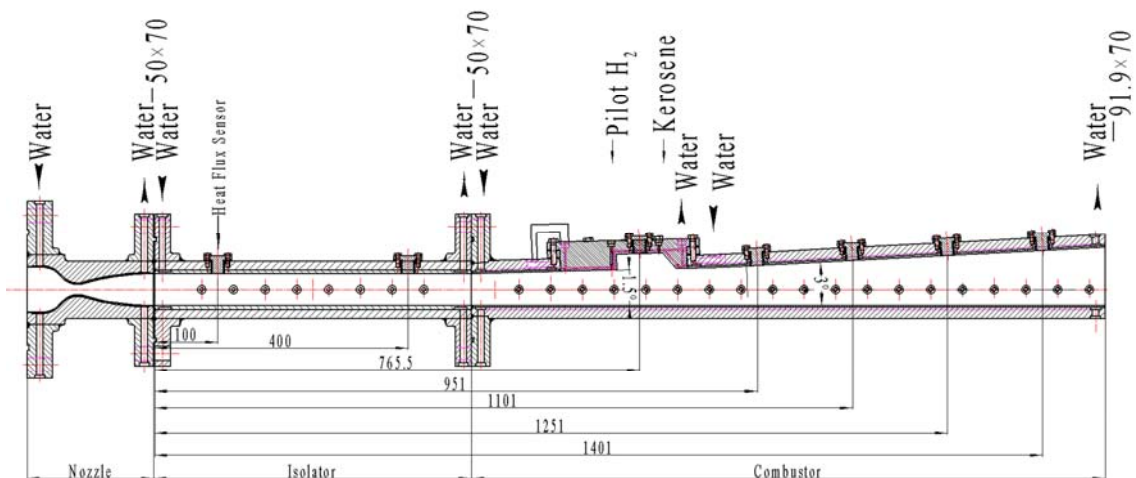


Fig. 21 Sketch of the water cooled supersonic model combustor.

Fig. 22 and Fig. 23 show the time histories of measured wall heat fluxes and temperatures during a single run at fuel equivalence ratio of 0.67, total temperature of 1650 K and total pressure of 1.4 MPa. To measure the wall heat fluxes without combustion, the liquid kerosene fuel was injected at the 20th second. It can be seen from the figures that both the heat fluxes and wall temperatures at all locations reach steady states after approximately 10 seconds. The outputs from the five sensors installed in combustion section climb to the second steady states after another 10 seconds when fuel was injected, while the outputs from the first two sensors installed in the isolator remain almost constant.

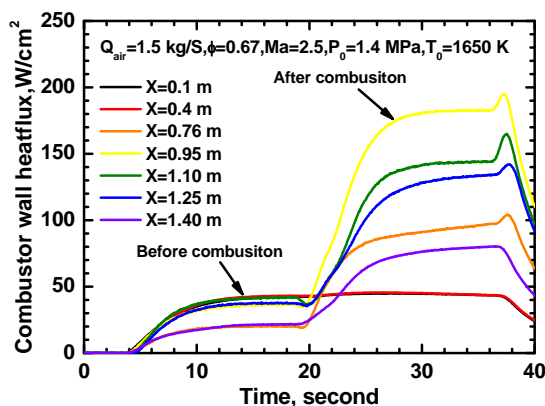


Fig. 22 Time histories of the wall heat fluxes along the combustor.

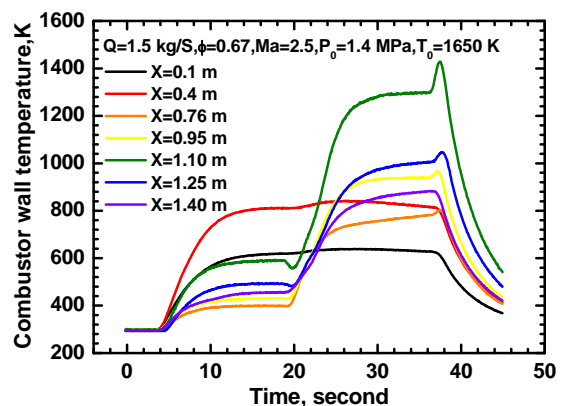


Fig. 23 Time histories of the wall temperatures along the combustor.

Fig. 24 compares the wall heat flux distributions at the 16th (no combustion) and 36th seconds (combustion). The maximum heat flux with combustion increases approximately 4-5 times. The peak heat flux appears just downstream the cavity. Fig. 25 shows the corresponding wall temperature distributions for the two cases. The wall temperatures with combustion is nearly twice as much as that without combustion in the combustion region. Most of the sensors survived after about 50 runs and the outputs showed very good repeatability.

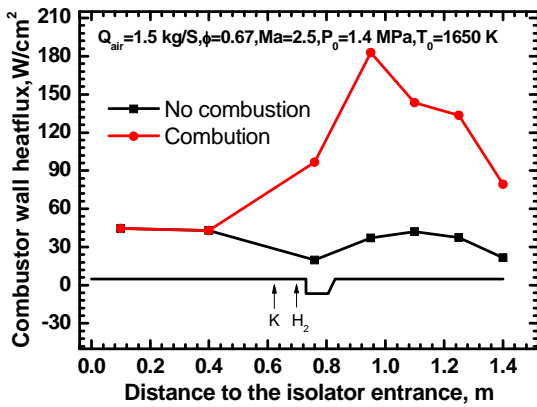


Fig. 24 Heat flux distributions along the combustor with and without combustion.

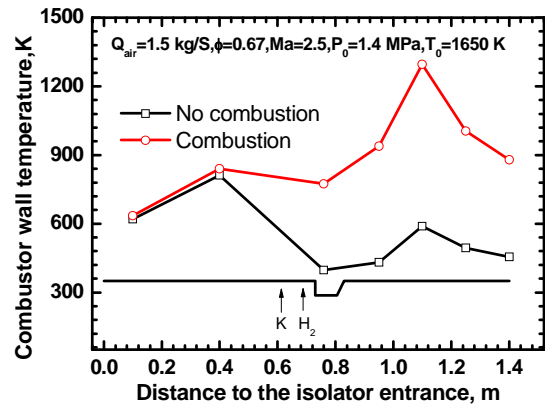


Fig. 25 Wall temperature distributions along the combustor with and without combustion.

Fig. 26 shows steady state heat flux distributions along the combustor without any combustion at different total temperatures of airflow. It can be seen that the wall heat flux increases with the total temperature of airflow.

Fig. 27 shows the heat flux distributions along the combustor with and without combustion at different air mass flows. It can be seen that the wall heat flux increases with mass flow for the similar air total temperature and fuel equivalence ratio.

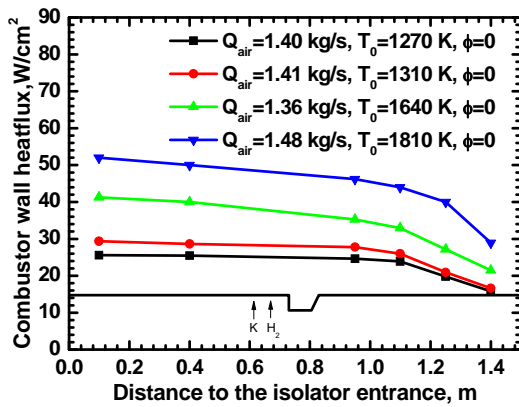


Fig. 26 Heat flux distributions without combustion at different air total temperatures.

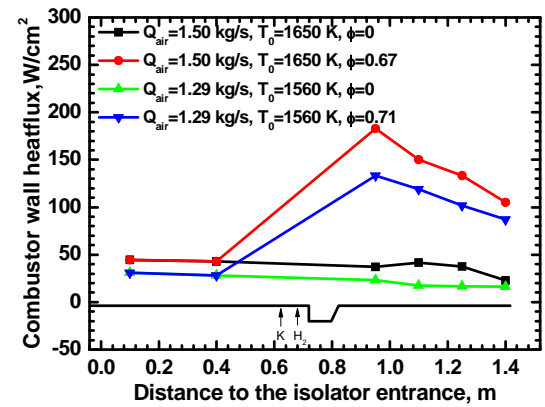


Fig. 27 Heat flux distributions at different air mass flow.

Fig. 28 shows the heat flux distributions along the combustor with and without combustion at different kerosene equivalence ratios (0.67 and 0.80). Fig. 29 shows the heat flux distributions along the combustor with and without combustion at different total temperatures of airflow. Under almost identical air mass flow and fuel equivalence ratio, the maximum heat flux increased approximately 50% when total temperature increased from 1600 K to 1900 K.

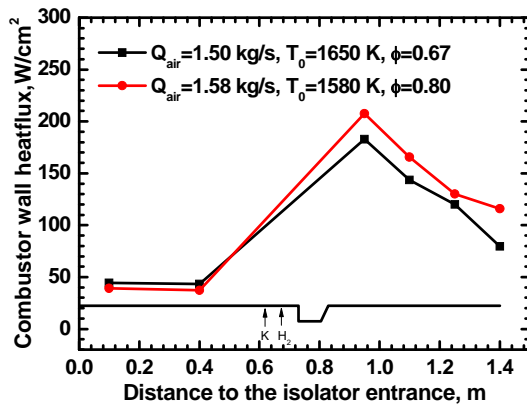


Fig. 28 Heat flux distributions at different fuel equivalence ratios.

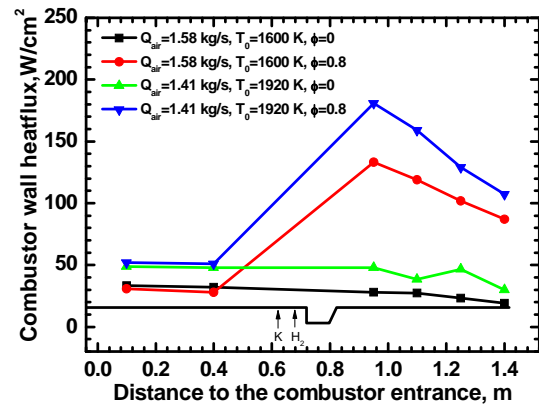


Fig. 29 Heat flux distributions with and without combustion at different air total temperatures.

VI. Conclusion

A water-cooled heat flux/wall temperature measurement technique has been developed based on the principle of Gardon heat-flux sensor. Heat resistance analysis has been used to design the thermal structure of the sensor. Numerical simulation of the heat conduction inside the sensor structure demonstrated that the output of the sensor was linearly proportional to the applied heat flux and a maximum heat flux of 400 W/cm² could be measured using this sensor. Sensor response time comparable to that of Gardon gauge was also obtained. Calibration processes using radiative and conductive heating sources were carried out and calibration curves of heat flux vs. voltage and wall temperature vs. heat flux were obtained. Calibration at large heat flux was carried out using a blackbody cavity. Effects of materials and structure on the sensor's responses have also been examined. Preliminary measurements inside a supersonic model combustor showed that the sensors developed in this work had fast time response and satisfactory reliability.

Acknowledgments

Current research program at the Chinese Academy of Sciences was supported by the National Natural Science Foundation of China under Contract No. 91016005 and 10621202. The authors would like to acknowledge Mr. J. Q. Wang, X. S. Wei, P. Huang, Y. Li and L. J. Meng for their technical support.

References

- ¹Ewing, J., Gifford, A., Hubble, D., Vlachos, P., Wicks, A. and Diller, T., "A direct-measurement thin-film heat flux sensor array", *Measurement Science & Technology*, Vol. 21, NO. 10, 2010, pp. 1-8.
- ²Kidd, C. T. and Adams, J. C., "Fast-response heat-flux sensor for measurement commonality in hypersonic wind tunnels", *Journal of Spacecraft and Rockets*, Vol. 38, NO. 5, 2001, pp. 719-729.
- ³Epstein, A. H., Guenette, G. R., Norton, R. J. G. and Cao, Y. H., "High-Frequency Response Heat-Flux Gauge", *Review of Scientific Instruments*, Vol. 57, NO. 4, 1986, pp. 639-649.
- ⁴Hager, N. E., "Thin Foil Heat Meter", *Review of Scientific Instruments*, Vol. 36, NO. 11, 1965, pp. 1564-1570.
- ⁵Lohle, S., Battaglia, J. L., Jullien, P., van Ootegem, B., Couzi, J. and Lasserre, J. P., "Improvement of high heat flux measurement using a null-point calorimeter", *Journal of Spacecraft and Rockets*, Vol. 45, NO. 1, 2008, pp. 76-81.
- ⁶George, W. K., Rae, W. J. and Woodward, S. H., "An evaluation of analog and numerical techniques for unsteady heat transfer measurement with thin-film gauges in transient facilities", *Experimental Thermal and Fluid Science*, Vol. 4, NO. 3, 1991, pp. 333-342.
- ⁷Liebert, C. H., Holanda, R., Hippensteele, S. A. and Andracchio, C. A., "HIGH-TEMPERATURE THERMOCOUPLE AND HEAT-FLUX GAUGE USING A UNIQUE THIN FILM-HARDWARE HOT JUNCTION", *Journal of Engineering for Gas Turbines and Power-Transactions of the Asme*, Vol. 107, NO. 4, 1985, pp. 938-944.
- ⁸Jan, M. S., Sebastian, K. and Klaus, H., "Ground Testing of the HyShot II Scramjet Configuration in HEG", AIAA 2008-2547, 2008.

- ⁹Gardner, A. D., Hannemann, K., Paull, A. and Steelant, J., "Ground testing of the HyShot supersonic combustion flight experiment in HEG", *Shock Waves, Vols 1 and 2, Proceedings*, Vol. NO. 2005, pp. 329-334.
- ¹⁰Ferriere, A. and Rivoire, B., "An instrument for measuring concentrated solar-radiation: A photo-sensor interfaced with an integrating sphere", *Solar Energy*, Vol. 72, NO. 3, 2002, pp. 187-193.
- ¹¹Ballestrin, J., Rodriguez-Alonso, M., Rodriguez, J., Canadas, I., Barbero, F. J., Langley, L. W. and Barnes, A., "Calibration of high-heat-flux sensors in a solar furnace", *Metrologia*, Vol. 43, NO. 6, 2006, pp. 495-500.
- ¹²Filtz, J. R., Valin, T., Hameury, J. and Dubard, J., "New Vacuum Blackbody Cavity for Heat Flux Meter Calibration", *International Journal of Thermophysics*, Vol. 30, NO. 1, 2009, pp. 236-248.
- ¹³Holmberg, D., Steckler, K., Womeldorf, C. and Grosshandler, W., "Facility for calibrating heat flux sensors in a convective environment," *Proceedings of the 1997 ASME International Mechanical Engineering Congress and Exposition, November 16, 1997 - November 21, 1997*, Dallas, TX, USA, 1997, pp. 165-171.
- ¹⁴Holmberg, D. G., Womeldorf, C. A. and Grosshandler, W. L., "Design and uncertainty analysis of a second-generation convective heat flux calibration facility," *Heat Transfer Division - 1999 (The ASME International Mechanical Engineering Congress and Exposition), November 14, 1999 - November 19, 1999*, Nashville, TN, USA, 1999, pp. 65-70.
- ¹⁵Grosshandler, W. L. and Blackburn, D., "Development of a high flux conduction calibration apparatus," *Proceedings of the 1997 ASME International Mechanical Engineering Congress and Exposition, November 16, 1997 - November 21, 1997*, Dallas, TX, USA, 1997, pp. 153-158.
- ¹⁶Murthy, A. V., Tsai, B. K. and Gibson, C. E., "Calibration of high heat flux sensors at NIST", *Journal of Research of the National Institute of Standards and Technology*, Vol. 102, NO. 4, 1997, pp. 479-488.
- ¹⁷Murthy, A. V., Tsai, B. K. and Saunders, R. D., "Radiative calibration of heat flux sensors at NIST - an overview," *Proceedings of the 1997 ASME International Mechanical Engineering Congress and Exposition, November 16, 1997 - November 21, 1997*, Dallas, TX, USA, 1997, pp. 159-164.
- ¹⁸Murthy, A. V., Tsai, B. K. and Saunders, R. D., "High-heat-flux sensor calibration using black-body radiation", *Metrologia*, Vol. 35, NO. Compendex, 1998, pp. 501-504.
- ¹⁹Murthy, A. V., Tsai, B. K. and Saunders, R. D., "Comparative calibration of heat flux sensors in two blackbody facilities", *Journal of Research of the National Institute of Standards and Technology*, Vol. 104, NO. 5, 1999, pp. 487-494.
- ²⁰Murthy, A. V., Tsai, B. K. and Saunders, R. D., "Radiative calibration of heat-flux sensors at NIST: Facilities and techniques", *Journal of Research of the National Institute of Standards and Technology*, Vol. 105, NO. 2, 2000, pp. 293-305.
- ²¹Murthy, A. V., Tsai, B. K. and Saunders, R. D., "Transfer calibration validation tests on a heat flux sensor in the 51 mm high-temperature blackbody", *Journal of Research of the National Institute of Standards and Technology*, Vol. 106, NO. 5, 2001, pp. 823-831.
- ²²Tsai, B., Gibson, C., Murthy, A., Early, E., Dewitt, D., and Saunders, R., *Heat-Flux Sensor Calibration*, U.S. Department of Commerce Technology Administration, National Institute of Standards and Technology, NIST Special Publication 250-65, 2004, pp.3-14.
- ²³Murthy, A. V., Prokhorov, A. V. and DeWitt, D. P., "High heat-flux sensor calibration: A Monte Carlo modeling", *Journal of Thermophysics and Heat Transfer*, Vol. 18, NO. 3, 2004, pp. 333-341.
- ²⁴Murthy, A. V., Fraser, G. T. and DeWitt, D. P., "Experimental in-cavity radiative calibration of high-heat-flux meters", *Journal of Thermophysics and Heat Transfer*, Vol. 20, NO. 2, 2006, pp. 327-335.
- ²⁵Abdelmessih, A. N. and Horn, T. J., "Experimental and computational characterization of high heat fluxes during transient blackbody calibrations", *Journal of Heat Transfer*, Vol. 132, NO. Compendex, 2010, pp. 1-13.
- ²⁶Gardon, R., "An Instrument for the Direct Measurement of Intense Thermal Radiation", *Review of Scientific Instruments*, Vol. 24, NO. 5, 1953, pp. 366-370.
- ²⁷International standard, IEC, Thermocouple-Part 1: Reference tables, IEC584-1.